

# DNA Methylome and Transcriptome Alterations in High Glucose-Induced Diabetic Nephropathy Cellular Model and Identification of Novel Targets for Treatment by Tanshinone IIA

Wenji Li,<sup>†,‡,§,⊥</sup> Davit Sargsyan,<sup>§,||,⊥</sup> Renyi Wu,<sup>§</sup> Shanyi Li,<sup>§,||</sup> Lujing Wang,<sup>§,||</sup> David Cheng,<sup>§,||</sup> and Ah-Ng Kong<sup>\*,§,¶</sup>

<sup>†</sup>Institute of Translational Medicine, Medical College and <sup>‡</sup>Jiangsu Key laboratory of integrated traditional Chinese and Western Medicine for prevention and treatment of Senile Diseases, Yangzhou University, Yangzhou 225001, P. R. China

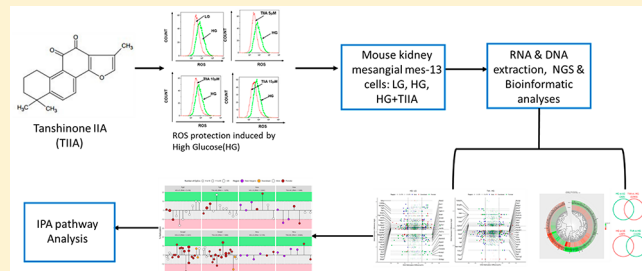
<sup>§</sup>Department of Pharmaceutics, Ernest Mario School of Pharmacy, Rutgers, The State University of New Jersey, 160 Frelinghuysen Road, Piscataway, New Jersey 08854, United States

<sup>||</sup>Graduate Program in Pharmaceutical Sciences, Ernest Mario School of Pharmacy, The State University of New Jersey, Piscataway, New Jersey 08854, United States

## Supporting Information

**ABSTRACT:** Diabetic nephropathy (DN) is a diabetes complication that comes from overactivation of Renin-Angiotensin System, excessive pro-inflammatory factors, reactive oxygen species (ROS) overproduction, and potential epigenetic changes. Tanshinone IIA (TIIA), a diterpene quinone phytochemical, has been shown to possess powerful antioxidant, anti-inflammatory, epigenetics, and protective effects against different diseases including DN by inhibiting ROS induced by high glucose (HG). However, epigenomic and transcriptomic study of DN and the protective effect of TIIA are lacking. In this study, next-generation sequencing of

RNA and DNA methylation profiles on the potential underlying mechanisms of a DN model in mouse kidney mesangial mes13 cells challenged with HG and treatment with TIIA were conducted. Bioinformatic analysis coupled with Ingenuity Pathway analysis of RNA-seq was performed, and 1780 genes from HG/LG and 1416 genes from TIIA/HG were significantly altered. Several pro-inflammatory pathways like leukotriene biosynthesis and eicosanoid signaling pathways were activated by HG stimulation, while TIIA treatment would enhance glutathione-mediated detoxification pathway to overcome the excess oxidative stress and inflammation triggered by HG. Combination analysis of RNA-seq and Methyl-seq data sets, DNA methylation, and RNA expression of a list of DN associated genes, *Nmu*, *Fgl2*, *Glo*, and *Knip2*, were found to be altered in HG-induced mes13 DN model, and TIIA treatment would effectively restore the alterations. Taken together, these findings provide novel insights into the understanding of how epigenetic/epigenomic modifications could affect the progression of DN and the potential preventive effect of TIIA in DN.



## 1. INTRODUCTION

Diabetic nephropathy (DN) manifested glomerular hyperfiltration and proteinuria in function, and renal hypertrophy, basement membrane thickening, extracellular matrix (ECM) accumulation, glomerulosclerosis, and interstitial fibrosis in histology and, finally, developed into renal failure.<sup>1</sup> Pathological factors attributed to development of DN were acknowledged to be a complexation of overactivation of Renin-Angiotensin System, excessive proinflammatory factors, reactive oxygen species (ROS) overproduction, and epigenetic changes.<sup>2–4</sup>

Among them, ROS overproduction played an important role in inducing apoptosis and kidney cell damage upon high glucose (HG) stimulations.<sup>5,6</sup> Multiple kidney cells were found to generate excessive ROS by stimulation of high glucose.<sup>7,8</sup> Overexpression of proinflammatory factors, such as trans-

forming growth factor- $\beta$ 1 (TGF- $\beta$ 1), has proved to be highly associated with ECM accumulation and glomerulosclerosis.<sup>9</sup> Overactivation of TGF- $\beta$ 1 would induce excessive ROS, which will in turn enhance the level of TGF- $\beta$ 1 and worsen the condition of DN.<sup>10</sup>

Nuclear factor erythroid 2-related factor 2 (Nrf2), one of the most important cellular defense mechanisms with the ability to modulate many phase II detoxifying enzymes by binding to antioxidant response element (ARE) of those genes and maintain cellular redox homeostasis,<sup>11</sup> has shown to be vital in regulating the antioxidative stress response and is essential for the anti-inflammatory response in many clinical and preclinical studies.<sup>12</sup> Accumulating data suggest that many dietary

Received: March 18, 2019

Published: September 5, 2019

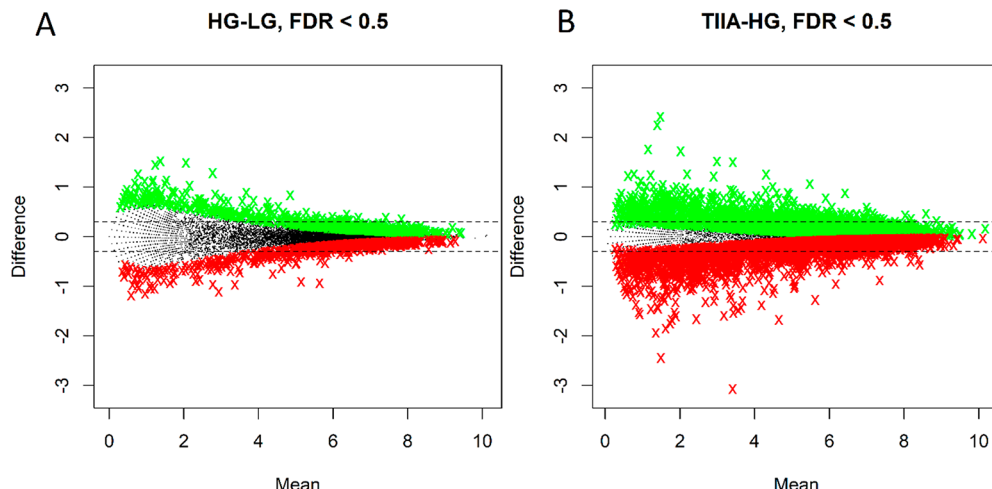


**Figure 1.** MA plots of Fragments Per Million mapped fragments (FPM)-normalized gene expressions (log<sub>2</sub> means vs log<sub>2</sub> difference) for the two comparisons: HG vs LG (A) and TIIA in HG vs HG only (B). The two horizontal dotted lines correspond to log<sub>2</sub> differences of  $\pm 0.3$ . The colored symbols correspond to upregulated (green) and downregulated (red) genes with *q*-values of 0.5 or less.

phytochemicals can induce Nrf2-mediated antioxidant/anti-inflammatory signaling pathways.<sup>13</sup> Hence many of them are used for inhibiting DN.<sup>14–16</sup>

Tanshinone IIA (TIIA), a diterpene quinone phytochemical isolated from *Salvia miltiorrhiza*, has a long history of application for cardiovascular disease.<sup>17</sup> Notably, TIIA can suppress ROS and inflammation through activating Nrf2 pathway.<sup>18,19</sup> Besides cardioprotective effect, TIIA also possesses multiple pharmacological effects, including antioxidant,<sup>20</sup> anti-angiogenesis,<sup>21</sup> anti-inflammatory,<sup>22</sup> and neuro-protective effects,<sup>23</sup> which contributes to its diverse therapeutic spectrum including diabetes.<sup>24,25</sup> TIIA exhibits protective effects on both acute kidney injury<sup>26,27</sup> and chronic renal disorders.<sup>28,29</sup>

However, there is very limited evidence of TIIA on DN, which all used rat cells or streptozotocin (STZ) induced type I DN rat model.<sup>24,30,31</sup> In addition, the underlying mechanism of action is not clear. A systematic screening for targets of TIIA effects on DN is highly needed.

More and more emerging evidence indicates epigenetic changes, including DNA methylation, histone post-translational modifications (PTMs), and noncoding RNA-mediated post-transcriptional alterations, are closely related to DN.<sup>32–34</sup> Next-generation sequencing (NGS) on whole genome or epigenome would provide systematic means in analyzing new biomarkers associated with DN, which will provide a novel target for treatment. NGS results including RNA-seq and noncoding RNA-seq began to reveal the novel DN associated biomarkers genome wide.<sup>35,36</sup> However, there lacks whole DNA methylome especially whole methylome and transcriptome synergistic investigations into the pathological changes of DN. This paper will report our work on DNA methyl-seq and mRNA-seq coalterations using a high-glucose induced mouse kidney mesangial cell model that represents diabetes *in vitro*. The NGS results comparison between high glucose, low glucose, and TIIA will also provide identification of novel targets for diabetic nephropathy and treatment by TIIA.

## 2. MATERIAL AND METHODS

### 2.1. Materials.

Dulbecco's modified Eagle's medium, fetal bovine serum (FBS), penicillin-streptomycin (10 000 U/ml), puromycin,

**Table 1. Real-Time q-PCR Primers Information of Validated Genes of Interest**

genes	primer sequence (5'-3')	amplicon size (bp)
<i>Nmu</i>	F: CTCAAAGATTGCAGCCAGAAC R: ATCACTATACGGCAAAGCTCC	87
<i>Fgl2</i>	F: AAGTGTCCAAGTGTCCCAG R: TGCTGTTCTGTGATCAGGG	101
<i>Gulo</i>	F: AACTGGCGGAAGACCTATG R: GATGTCGAAGGCAGTGG	105
<i>Kcnip2</i>	F: GAGAGTTGTCCGAATCCCG R: TCTCTGCGTGTGAACCTGG	106
<i>β-actin</i>	F: ACCTTCTACAATGAGCTGCG R: CTGGATGGCTACGTACATGG	106

versene, and trypsin-ethylenediaminetetraacetic acid (EDTA) were supplied by Gibco. TIIA and dimethyl sulfoxide (DMSO) were purchased from Sigma-Aldrich.

**2.2. Methods.** *2.2.1. Mouse Mesangial Cell Culture.* SV40 MES 13 mouse kidney mesangial cells were obtained from the American Type Culture Collection and maintained in Dulbecco's modified Eagle's medium (Gibco; Thermo Fisher Scientific, Inc.) with 14 mM 2-[4-(2-hydroxyethyl)piperazin-1-yl]ethanesulfonic acid (HEPES) (Gibco; Thermo Fisher Scientific, Inc.) and 5% FBS (Gibco; Thermo Fisher Scientific, Inc.) at 37 °C with 5% CO<sub>2</sub>. Mesangial cells were seeded at 1 × 10<sup>3</sup> cells/10 cm dish and were treated with serum-free medium for 1 d followed by 0.1% DMSO in 30 mM D-glucose (HG), 0.1% DMSO in 5.5 mM D-glucose + 24.5 mM D-mannitol (isotonic control, low glucose (LG)), or TIIA (5,10, 15 μM dissolved in 0.1% DMSO in LG) for 5 d.

*2.2.2. Intracellular ROS Detection.* CM-H2DCFDA (Invitrogen) was used as the probe. Mes-13 cells were treated with 0.1% DMSO in LG, 0.1% DMSO in HG or TIIA (5,10, 15 μM in 0.1% DMSO in HG) for 48 h. The cells were grown to 90% confluence, washed with PBS, and then harvested using trypsinization, according to the manufacturer's protocol. The cells were then washed four times and incubated with 10 μM CM-H2DCFDA for 45 min at 37 °C in a relatively high humidity (95%) atmosphere containing a controlled level of CO<sub>2</sub> (5%) in the dark. Finally, cell-associated mean fluorescent intensity was measured by flow cytometry in FL1 channel excitation, and emission wavelengths were 488 and 525 nm, respectively.

*2.2.3. Total RNA/DNA Extraction, Library Preparation, RNA-seq and methyl-seq.* Total RNA and DNA was extracted from SV40 MES 13 mouse kidney mesangial cells from LG, HG, and TIIA groups

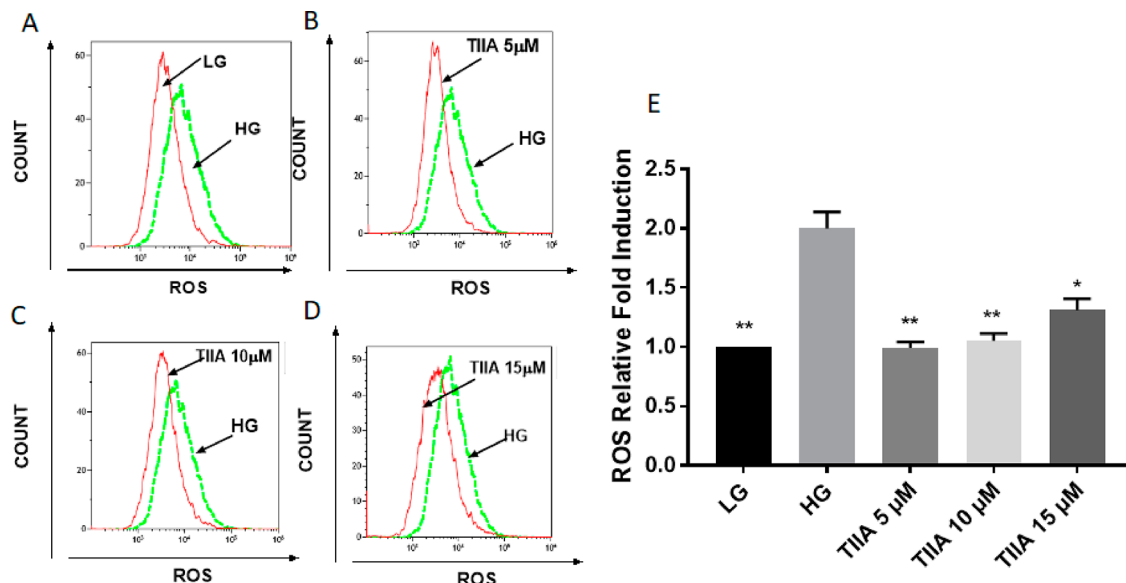


**Figure 2.** Effects of TIIA on production of intracellular ROS induced by 2 d treatment of HG In mouse kidney mes-13 cells via flow cytometry. Two-day treatment of HG-induced increase of intracellular ROS damage compared with LG group (A), cotreatment of 5  $\mu$ M TIIA (B), 10  $\mu$ M TIIA (C), and 15  $\mu$ M TIIA (D) could protect mes-13 cells against ROS damage from HG. Relative ROS fold change normalized by LG (E) are expressed as means  $\pm$  std for three independent replicates, and significant ( $p < 0.05$ , \*;  $p < 0.01$ , \*\*) differences compared with HG are indicated.

using the AllPrep DNA/RNA Mini Kit (Qiagen). The quality and quantity of the extracted RNA and DNA samples were determined with an Agilent 2100 Bioanalyzer and NanoDrop, respectively. A total of three RNA and DNA pooled samples from each group were sent to RUCDR for library preparation and sequencing. Briefly, the library of RNA-seq was constructed using the Illumina TruSeq RNA preparation kit (Illumina) according to the manufacturer's manual. Samples were sequenced on the Illumina NextSeq 500 instrument with 50–75 bp paired-end reads, to a minimum depth of 30 million reads per sample. The DNA samples were further processed using an Agilent Mouse SureSelect Methyl-seq Target Enrichment System (Agilent Technologies) to enrich the targets of interest. Briefly, 1  $\mu$ g of genomic DNA was fragmented to the size of ~200 bp by sonication and then hybridized with the Agilent SureSelect Mouse Methyl-seq probes, which targeted 109 MB of the mouse genome, or 3.3 million CpG sites, followed by bisulfite treatment and PCR amplification and then sequenced on an Illumina NextSeq 500 instrument with 76 bp single-end reads, generating 34–47 million reads per sample.

**2.2.4. Data Analysis.** Sequencing data quality was checked using FastQC 0.11.2 software.<sup>37</sup> Linux-based bioinformatics software packages Sequencing Alignment/Map tools (SAMtools)<sup>38</sup> and hierarchical indexing for spliced alignment of transcripts (HISAT-2)<sup>39</sup> were used to sort, deduplicate, index, and align reads in RNA sequencing files. DNA methylation data were processed with Bismark tool.<sup>40</sup> All reads were aligned to the mouse reference genome (mm9.2). R 3.5.1 (R Core Team)<sup>41</sup> was used for all downstream statistical analysis and visualization of RNA and DNA sequencing data.

**2.2.5. Differential Gene Expression Analysis.** Total of 24 421 genes were mapped. Genes with low counts (less than 20 counts in all samples combined) were removed from the analysis. The remaining 13 954 genes were further examined. Two comparisons—high glucose versus low glucose, and TIIA in HG vs HG only—were done using an R package DEGSeq<sup>42</sup> to identify differentially expressed genes. The genes with the log<sub>2</sub> difference of at least 0.3 and filtered by  $q$ -values as defined by Storey et al.<sup>43</sup> were selected. The MA plots (log differences vs log means) for the two comparisons are shown in Figure 1. The RNA expression patterns of the selected genes were further explored to isolate genes that were affected by the HG treatment but restored by the TIIA.

**2.2.6. SureSelect Methyl-seq Analysis.** After alignment, DMRfindr (version 0.1) was used to extract methylation counts and cluster

CpG sites into Differential Methylation Regions (DMRs).<sup>44</sup> Each DMR was defined to contain at least three CpG sites. Genomic annotation was performed with ChIPseeker (version 1.10.3) in R.<sup>45</sup> To examine the associations of DNA methylation and the downstream RNA expression, the differences in percent methylation and RNA expressions for the genes selected in the RNA-seq analysis were plotted against each other. The genes that exhibited DNA hypermethylation in promoter and RNA downregulation or DNA hypomethylation in promoter and RNA upregulation were selected as genes of interest for further analysis.

**2.2.7. Ingenuity Pathway Analysis (IPA) Analysis.** Isoforms with log<sub>2</sub> ratios greater than 0.3 or less than -0.3 and filtered by  $q$ -values were subjected to Ingenuity Pathway Analysis (IPA 4.0, Ingenuity Systems, [www.Ingenuity.com](http://www.Ingenuity.com)). The input isoforms were mapped to IPA's database, and the top related genes, relevant biological functions, diseases, and canonical pathways related to HG-induced pathological changes and TIIA interventions were identified.

**2.2.8. Quantitative Polymerase Chain Reaction (qPCR) Validation of Genes of Interest.** qPCR was used to validate the expression trends of selected genes of interest identified by methyl-seq and RNA-seq. First-strand cDNA from isolated 300 ng mRNA from pooled samples was synthesized using TaqMan Reverse Transcription reagents (Applied Biosystems). qPCR was performed using a QuantStudio 5 Real-Time PCR System (Applied Biosystems) with SYBR Green PCR Master Mix (Applied Biosystems) with the qPCR primers listed in Table 1. The gene expression fold changes were normalized to the expression of  $\beta$ -actin using the  $2^{\Delta\Delta CT}$  method (RQ values). The gene expressions from HG group were normalized to 1, and the relative fold changes were obtained from the comparison between the other two groups to HG group. All the primers were designed and ordered from Integrated DNA Technologies (IDT).

**2.2.9. Statistical Analysis.** The data are presented as the mean  $\pm$  standard deviation (std). One-way analysis of variance (ANOVA) test was performed to test for the differences between the mean RQ values of the three treatment groups, followed by a post hoc pairwise comparisons (Dunnett's test). Differences with  $p$ -values less than 0.05 were considered statistically significant.

### 3. RESULTS

#### TIIA Exerted Protection Effect on Intracellular Reactive Oxygen Species (ROS) Induced by High

**Table 2.** Top 50 Annotated Genes Showing the Highest log<sub>2</sub>-Fold Change in Either Direction in High-Glucose-Treated Group (HG) over Low-Glucose-Treated Group (LG), Ranked by log<sub>2</sub>-Fold Change

increased (HG/LG)		decreased (HG/LG)	
symbol	log <sub>2</sub> -fold change	symbol	log <sub>2</sub> -fold change
<i>Nmu</i>	4.129	<i>Zic2</i>	-4.626
<i>Them5</i>	3.959	<i>Gm14827</i>	-3.848
<i>Dhh</i>	3.766	<i>Lyz</i>	-3.848
<i>Hsd3b1</i>	3.659	<i>Nutm1</i>	-3.626
<i>Cd300a</i>	3.544	<i>Sh3bgr</i>	-3.626
<i>Cyp2ab1</i>	3.544	<i>Grin1</i>	-3.501
<i>Fbxl13</i>	3.544	<i>Gulo</i>	-3.041
<i>Insyn2</i>	3.544	<i>Kcnip2</i>	-3.041
<i>Arhgap6</i>	3.281	<i>Tssk2</i>	-3.041
<i>C130021I20Rik</i>	3.281	<i>C11orf98</i>	-2.848
<i>C4A/C4B</i>	3.281	<i>Hist2h2bf</i>	-2.848
<i>Dpep2</i>	3.281	<i>Il23r</i>	-2.848
<i>E130102H24Rik</i>	3.281	<i>Tnfrsf25</i>	-2.848
<i>Entpd1</i>	3.281	<i>Smyd1</i>	-2.742
<i>Pbld</i>	3.281	<i>Ankrd61</i>	-2.626
<i>Pga5</i>	3.281	<i>Aox4</i>	-2.626
<i>Scn1a</i>	3.281	<i>C11orf65</i>	-2.626
<i>Snora5c</i>	3.281	<i>Ephx4</i>	-2.626
<i>Zfp345 (includes others)</i>	3.281	<i>Fcer1g</i>	-2.626
<i>Kcnj15</i>	3.129	<i>Mir1191</i>	-2.626
<i>Obscn</i>	3.129	<i>Mir8091</i>	-2.626
<i>Cd59a</i>	2.959	<i>Npas3</i>	-2.626
<i>Hnf4a</i>	2.959	<i>Mamdc2</i>	-2.501
<i>Acsm2a</i>	2.766	<i>Myo7b</i>	-2.501
<i>Ces2f</i>	2.766	<i>Olf99</i>	-2.501
<i>Hpgds</i>	2.766	<i>C19orf66</i>	-2.363
<i>Islr2</i>	2.766	<i>Gng8</i>	-2.363
<i>Clk3</i>	2.766	<i>Mesp2</i>	-2.363
<i>Ldhd</i>	2.766	<i>Slc4a5</i>	-2.363
<i>Lipn</i>	2.766	<i>Bmp8b</i>	-2.157
<i>Mkl1nos</i>	2.766	<i>C1qtnf3</i>	-2.157
<i>Nckap5</i>	2.766	<i>Atp2a1</i>	-2.041
<i>Kiaa1324</i>	2.681	<i>Cd160</i>	-2.041
<i>Akap5</i>	2.544	<i>Ces1f</i>	-2.041
<i>Cfap45</i>	2.544	<i>Cyp4f12</i>	-2.041
<i>Chn1os3</i>	2.544	<i>Dusp13</i>	-2.041
<i>Cyp2j5</i>	2.544	<i>Epstil</i>	-2.041
<i>Cyp4f22</i>	2.544	<i>Gbp8</i>	-2.041
<i>Fam19a5</i>	2.544	<i>GJA4</i>	-2.041
<i>Gpr132</i>	2.544	<i>Mapk10</i>	-2.041
<i>Icam1</i>	2.544	<i>Mc1r</i>	-2.041
<i>Pknox2</i>	2.544	<i>Myo16</i>	-2.041
<i>Rab39b</i>	2.544	<i>Nrp</i>	-2.041
<i>Slc22a6</i>	2.544	<i>Serpib9f (includes others)</i>	-2.041
<i>Sox21</i>	2.544	<i>Slc23a1</i>	-2.041
<i>Tcp11</i>	2.544	<i>Tmem266</i>	-2.041
<i>Fgl2</i>	2.418	<i>Tmod1</i>	-2.041
<i>Gm19589</i>	2.418	<i>Wfdc3</i>	-2.041
<i>4930447K03Rik</i>	2.281	<i>Ccdc116</i>	-1.967

**Glucose.** In mouse kidney mes-13 cells, 2 d treatment of HG will induce a twofold increase of intracellular ROS damage comparing with low glucose group (Figure 2A,E), while cotreatment of TIIA (5, 10, and 15  $\mu$ M) (Figure 2B–E) could

**Table 3.** Top 50 Annotated Genes Showing the Highest log<sub>2</sub>-Fold Change in Either Direction in 5  $\mu$ M TIIA Treated Group (TIIA) over HG, Ranked by log<sub>2</sub>-Fold Change

increased (TIIA/HG)		decreased (TIIA/HG)	
symbol	log <sub>2</sub> -fold change	symbol	log <sub>2</sub> -fold change
<i>Gsta5</i>	4.727	<i>Lcn2</i>	-4.756
<i>Gsta1</i>	4.523	<i>Ace2</i>	-4.586
<i>Sh3bgr</i>	3.999	<i>Gm19589</i>	-4.46
<i>Ugt2b28</i>	3.999	<i>Hspa12a</i>	-4.46
<i>Il23r</i>	3.906	<i>Iigp1</i>	-4.46
<i>Htra3</i>	3.806	<i>Steap4</i>	-4.393
<i>Kchn4</i>	3.806	<i>Ccdc33</i>	-4.323
<i>Adam32</i>	3.584	<i>Abca12</i>	-4.171
<i>Snora2b</i>	3.584	<i>Lpl</i>	-4.001
<i>Ly6a (includes others)</i>	3.321	<i>Them5</i>	-4.001
<i>Lyz</i>	3.321	<i>Trim30a/Trim30d</i>	-3.908
<i>Msc</i>	3.321	<i>MS4a10</i>	-3.808
<i>Nostrin</i>	3.321	<i>Dpt</i>	-3.701
<i>Nyx</i>	3.321	<i>S100g</i>	-3.701
<i>Tnfrsf25</i>	2.806	<i>Cd300a</i>	-3.586
<i>Bmp8b</i>	2.584	<i>Cyp4f22</i>	-3.586
<i>Fcer1g</i>	2.584	<i>Ify4</i>	-3.586
<i>Itgb2l</i>	2.584	<i>Ly6a (includes others)</i>	-3.586
<i>Nkx6-3</i>	2.584	<i>Nrl13</i>	-3.586
<i>Wscd2</i>	2.584	<i>Tll1</i>	-3.586
<i>Dusp13</i>	2.458	<i>Ube2ql1</i>	-3.586
<i>Rorc</i>	2.458	<i>Nad+</i>	-3.481
<i>Gm4432</i>	2.414	<i>Cccdc160</i>	-3.46
<i>Rapsn</i>	2.368	<i>Gli2</i>	-3.323
<i>Chrm1</i>	2.321	<i>mir-761</i>	-3.323
<i>Dpf3</i>	2.321	<i>Obscn</i>	-3.171
<i>Gja4</i>	2.321	<i>Pla2r1</i>	-3.171
<i>Mesp2</i>	2.321	<i>Rcsd1</i>	-3.171
<i>Mir1191</i>	2.321	<i>3830432H09rik</i>	-3.001
<i>Mpz</i>	2.321	<i>A630001g21rik</i>	-3.001
<i>Nalcn</i>	2.321	<i>Snord19</i>	-3.001
<i>Slc23a1</i>	2.321	<i>Inmt</i>	-2.971
<i>Slc4a5</i>	2.321	<i>Ccl5</i>	-2.808
<i>Snora43</i>	2.321	<i>Histih2bi</i>	-2.808
<i>Tssk2</i>	2.321	<i>Phf24</i>	-2.808
<i>Wfdc3</i>	2.321	<i>Agt</i>	-2.645
<i>Snora23</i>	2.169	<i>Ferm1</i>	-2.586
<i>Tfr2</i>	2.169	<i>Galnt18</i>	-2.586
<i>Ankrd61</i>	2.114	<i>Gpr132</i>	-2.586
<i>Ankrd63</i>	1.999	<i>Il23a</i>	-2.586
<i>Arsj</i>	1.999	<i>Pde11a</i>	-2.586
<i>Atp2a1</i>	1.999	<i>Plxnc1</i>	-2.586
<i>C11orf98</i>	1.999	<i>Prdm1</i>	-2.586
<i>C19orf66</i>	1.999	<i>Rbp4</i>	-2.586
<i>Ephx4</i>	1.999	<i>Timd2</i>	-2.586
<i>Gng8</i>	1.999	<i>Ttyh1</i>	-2.586
<i>Grin1</i>	1.999	<i>Tulp2</i>	-2.586
<i>Gulo</i>	1.999	<i>Hist1h2al</i>	-2.504
<i>Kcnip2</i>	1.999	<i>Rsd2</i>	-2.475
<i>Kl</i>	1.999	<i>Kiaa1324</i>	-2.46

protect mes-13 cells against ROS damage by HG. Excessive ROS is highly associated with apoptosis and kidney cell damage upon HG stimulations in DN,<sup>5,6</sup> and TIIA treatment has shown a very promising reversal efficacy, especially at 5  $\mu$ M

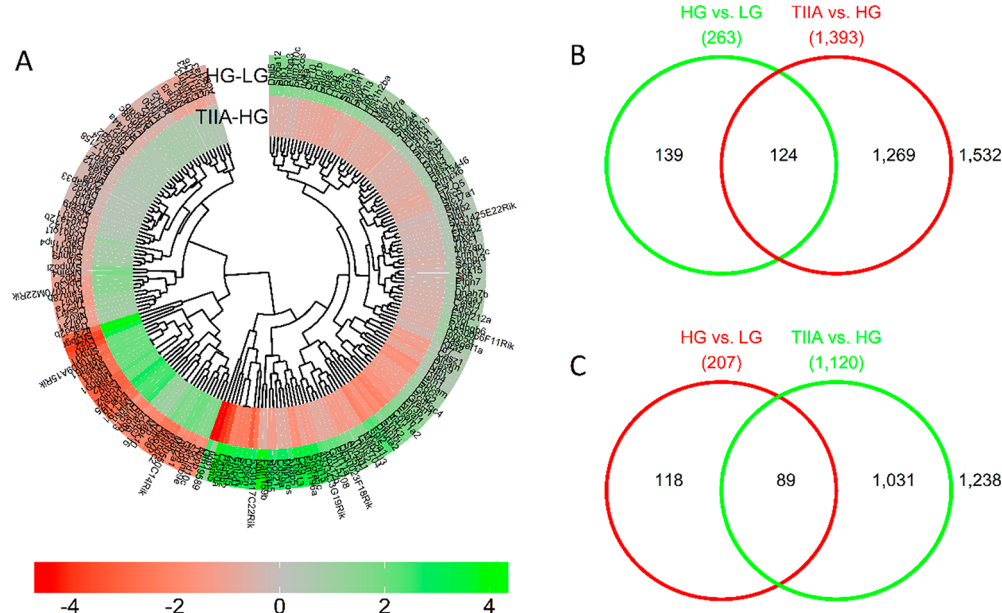


**Figure 3.** Overview of the differentially expressed genes (absolute log<sub>2</sub> difference greater than 0.3) in the two comparisons: HG vs LG and TIIA vs HG. The heatmap of differentially expressed genes (A) shows 124 genes upregulated by HG and downregulated by TIIA (B), and 89 genes downregulated by HG and upregulated by TIIA(C).

concentration. Hence, in the following NGS study, we treated mes-13 cells at this concentration for 5 d to study the global epigenomics change induced by TIIA in preventing DN.

**Global Transcriptome Results Comparison.** Global gene expressions were ranked in the order of expression log<sub>2</sub>-fold change. 1780 genes from HG/LG and 1416 genes from TIIA/HG with the log<sub>2</sub> fold-change levels of 0.3 or more (both, positive and negative) were then used as an input to the IPA software. Top 50 annotated genes with the highest log<sub>2</sub>-fold change in either direction in HG over LG comparison and top 50 annotated genes with the highest log<sub>2</sub>-fold change in either direction in TIIA over HG were listed in Tables 2 and 3, respectively. Doughnut heatmap (Figure 3A) demonstrates the 213 overlapping genes with log<sub>2</sub>-fold changes greater than 0.3 and filtered by *q*-values that show reversal of the effect of HG treatment by TIIA. The detailed 213 differentially expressed genes in HG/LG and TIIA/HG comparisons are listed in Table S1. As indicated in the Venn diagrams, there are 263 genes increased in HG versus LG and 1393 genes decreased in TIIA versus HG. Among them, the same 124 genes both increased in HG over LG and decreased in TIIA over HG (Figure 3B). There are 207 genes decreased in HG over LG and 1120 genes increased in TIIA over HG. Among them, same 89 genes both decreased in HG over LG and increased in TIIA over HG (Figure 3C). Those 124 overlapping genes from HG/LG and 89 from TIIA/HG that show the opposite trends in the comparisons were marked as candidates for the genes of interest.

**SureSelect Methyl-seq Analysis.** To understand the involvement of DNA methylation in DN, we used Agilent SureSelect Mouse Enrichment system to determine the single-base-resolution DNA methylation profiles of mouse kidney mesangial cells from LG, HG, and TIIA groups. This enrichment system focuses on the regions where methylation is known to impact gene regulation. It covers 109 MB of the mouse genome and targets 3.3 million CpG sites, which are the most complete content for methylation sequencing, including

cancer tissue specific DMRs, GENCODE promoters, CpG islands, shores and shelves, DNaseI hypersensitive sites, and RefGenes. It also delivers more information than methylation microarrays by detecting individual CpGs and reveals methylated regions undetected by reduced representation bisulfite sequencing (RRBS) and methylated DNA immunoprecipitation (MeDIP). Overall methylation is the average methylation across all DMRs. It is the ratio of the sum of all methylated hits over the total number of hits within each sample ( $\times 100\%$ ). A comparison of the methylation landscape across the treatments showed that overall methylation levels differed by the region but not by treatment; for example, methylation ratios were much lower in the promoter regions compared to body and downstream regions (Figure 4a). More than half of CpGs were located in the promoter ( $\leq 1$  kb) and the distal intragenic regions (Figure 4B). Average methylation levels were not significantly different between the treatment groups within each region (Figure 4C). This statistic of global methylation is not significantly different between treatments, because the majority of the DMRs were not significantly differentially methylated. However, at the individual gene level, we observed differences and found a small subset of DMRs in which changes in RNA expression of the corresponding genes correlated with the differences in CpG methylation. These genes are presented in the starburst plots (Figure 5). Heatmap showing methylation ratios of the promoter, gene body, and downstream regions of the comparisons between LG, HG, and TIIA from SureSelect Methyl-seq at the individual gene level are presented in Figure S1.

**Correlation of SureSelect Methyl-seq Results with RNA-seq Results.** Mounting evidence has suggested that the methylation status alteration of gene promoters, unlike other regions, caused reversed gene expression change: hypermethylation of coding or noncoding gene promoters correlates with the reduced expression of them, and hypomethylation correlates with increased expression.<sup>46</sup> On the basis of this notion, we prepared starburst figures to show the association

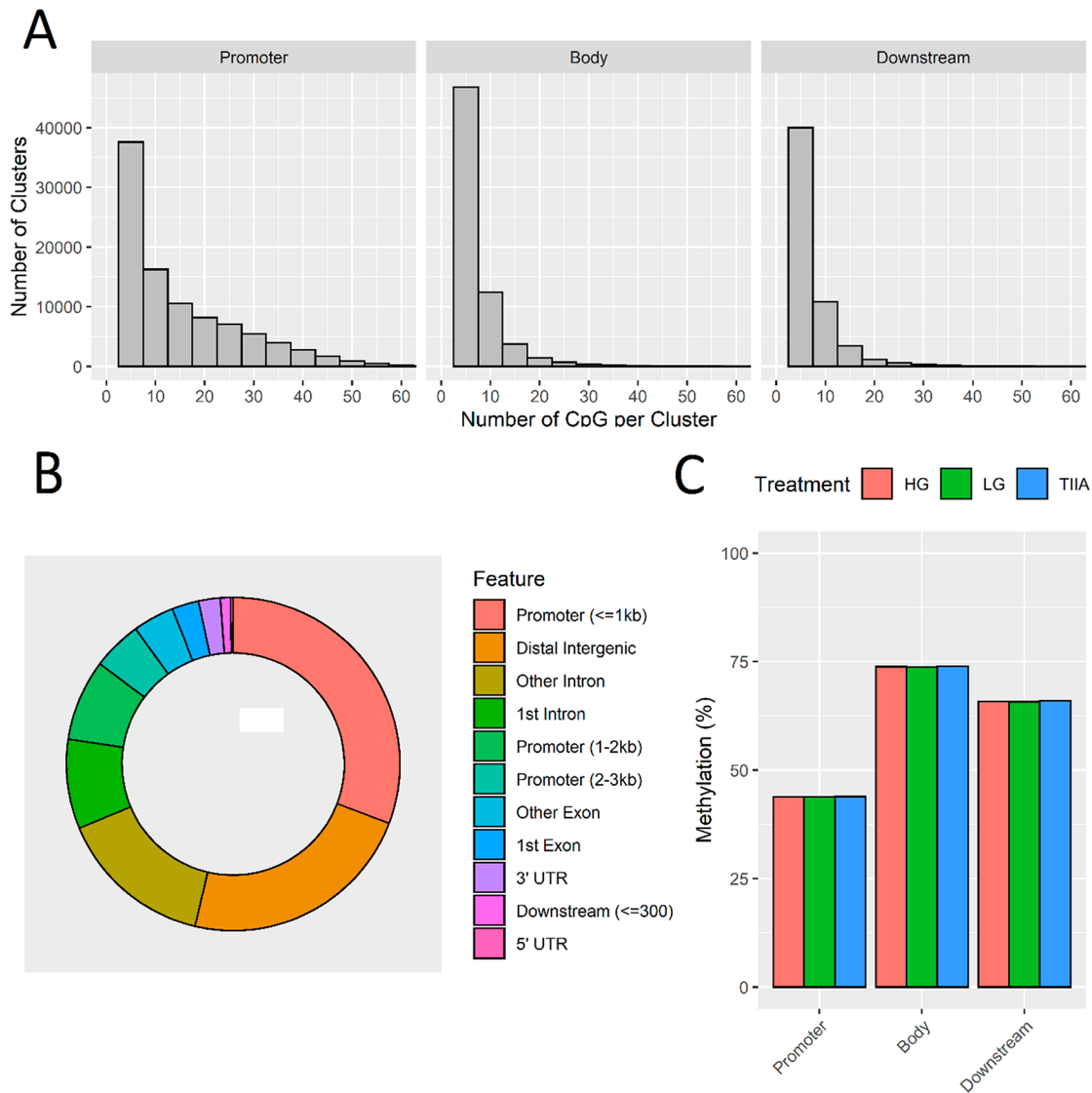


**Figure 4.** SureSelect Methyl-seq results. After alignment, DMRfinder was used to extract methylation counts and cluster CpG sites into DMRs. The cluster size is shown by region (A). More than half of CpGs were located in the promoter ( $\leq 1\text{ kb}$ ) and the distal intragenic regions (B). Average methylation levels were not significantly different between the treatment groups within each region (C).

between DNA methylation and gene expression of the 213 overlapping genes from the RNA-seq results (Figure 5A,B). The genes with green dots (corresponding to promoters) in the upper left and the lower right quadrants suggested reversed alteration of methylation in promoters with RNA expression levels. DNA methylation level differences of these genes along with the gene expression differences are presented as lollipop plots (Figure 7).

**Validation of Selected Gene Expression, which Shows Close Correlation between RNA-seq and methyl-seq by Quantitative Real-Time RT-PCR.** Genes of interest expression in HG were normalized to 1. In Figure 6, relative expression of *Gulo* and *Kcnip* were significantly decreased from 1.65 to 1 and from 1.29 to 1 in comparing LG with HG and increased from 1 to 1.54 and from 1 to 1.20 from HG to TIIA, respectively ( $p < 0.05$ ). Relative expression of *Fgl2* was significantly increased from 0.67 to 1 from LG group to HG group and decreased from 1 to 0.74 from HG to TIIA ( $p < 0.05$ ). The relative expression of *Nmu* was increased from 0.80 to 1 (from LG to HG) and decreased from 1 to 0.84

(from HG to TIIA). The above qPCR validation results correlate well with RNA-seq findings (Table 4).

**Lollipop Figures Show the Association between SureSelect methyl-seq and RNA-seq Results.** The lollipop plots (Figure 7A–H) provides in-depth understanding of RNA expression and DNA methylation difference within the HG/LG and TIIA/HG comparisons. The length of the stems corresponds to the methylation ratio, up or down orientation indicates the increase or decrease of methylation, the area of the bubbles correlates to the number of CpGs of each CpG cluster, and the color of the bubbles codes for the different methylation regions (distal intergenic region: purple; downstream: yellow; intron: white; promoter: red). RNA expressions of genes of interest are also listed in the figure. The lollipops figures are in good accordance with SureSelect methyl-seq results and demonstrate the association between DNA promoter methylation ratio and RNA expression. *Fgl2* and *Nmu* indicate a methylation ratio decrease in promoter region in HG/LG and the ratio increase in TIIA/HG. In addition, the genes expression from RNA-seq shows an

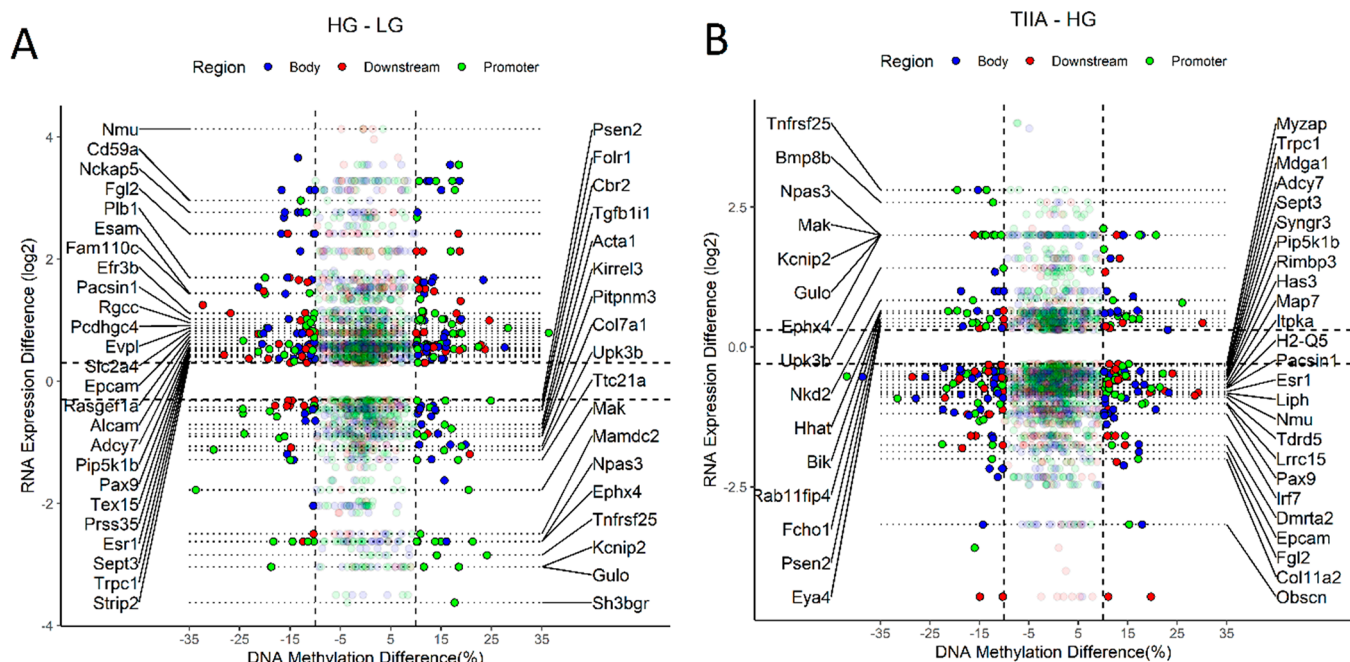


**Figure 5.** Starburst plot shows correlation between change in RNA expression level vs the change in methylation level in HG vs LG (A) and TIIA vs HG. The annotated genes had at least one CpG cluster with a change in methylation level negatively correlated with the change in RNA expression.

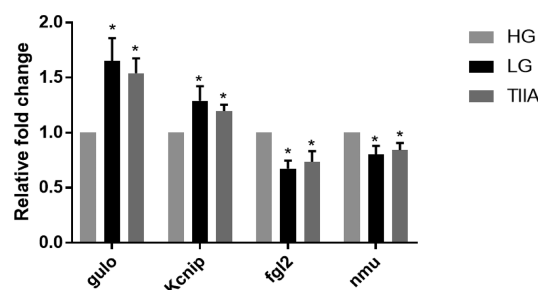


**Figure 6.** RNA qPCR validation for the genes of interest. The gene expressions from HG group were normalized to 1, and the relative fold changes were obtained from the comparison between the other two groups to HG group. All the data are presented are expressed as means  $\pm$  std for three independent replicates, and significant (\*,  $p < 0.05$ ) differences comparing with HG are indicated.

**Table 4. Correlation of DNA Promoter Methylation Ratio from SureSelect Methyl-seq and Fold Change of Gene Expression from RNA-seq for Genes of Interest**

genes of interest	DNA promoter methylation ratio of HG/LG	DNA promoter methylation ratio of TIIA/HG	fold change of expression in HG/LG from RNA-seq	fold change of expression in TIIA/HG from RNA-seq
Fgl2	-10.324	7.265	5.346	0.273
Gulo/ (GLO)	18.530	-14.526	0.121	3.997
Kcnip2/ KCIP2	11.567	-4.748	0.121	3.997
Nmu	-0.526	12.378	17.495	0.555

increase in HG/LG and decrease in TIIA/HG. *Gulo* and *Kcnip2* have opposite changes in DNA promoter methylation ratio and gene expression with *Fgl2* and *Nmu*. These results suggest treatment of TIIA can reverse HG influence in DNA

promoter methylation and gene expression in the four genes of interest.

#### 4. DISCUSSIONS AND CONCLUSIONS

**Top Differentially Canonical Pathways, Tox, and Diseases Influenced by HG and Treatment by TIIA Identified by IPA Analysis.** Figure 8 indicates the 10 most significant associated canonical pathways identified by IPA from all significant and reliable differentially expressed genes in HG versus LG (Figure 8a) and TIIA versus HG groups (Figure 8b) from mes-13 cells after 5 d treatment. In the top two significant associated pathways in the comparison group of HG versus LG, HG can induce both leukotriene biosynthesis and eicosanoid signaling, which are both highly related to enhance proinflammation factors like leukotrienes, prostaglandin, cyclooxygenases (COX-1 and COX-2), promote inflammation, and amplify immune response. Leukotrienes are proinflammatory metabolites of arachidonic acid (AA) that activate and amplify innate and adaptive immune responses.<sup>47</sup> They can induce leukocyte aggregation, activate phagocyte, and generate proinflammatory factors.<sup>48</sup> Four major types of eicosanoids, namely, prostaglandins, lipoxins, leukotrienes, and thromboxanes, are generated by AA through prostaglandin endoperoxide synthases or lipoxygenases.<sup>49</sup> Eicosanoids can modulate complicated oxidative response, inflammation, allergy, and carcinogenesis.<sup>50</sup> Our in vitro long-term HG treatment seems to be able to enhance oxidative stress and inflammation response in mouse kidney mesangial cells mainly via leukotriene biosynthesis and eicosanoid signaling pathway.

In the top two significant associated pathways in the comparison group of TIIA versus HG, TIIA can influence liver X receptor (LXR)/the retinoid X receptors (RXR) activation and enhance glutathione-mediated detoxification. LXR/RXR has a close relation with the regulation of metabolism of glucose, lipid, and cholesterol and inflammation.<sup>51</sup> Tripeptide glutathione (GSH) forms thioether conjugates with leuko-

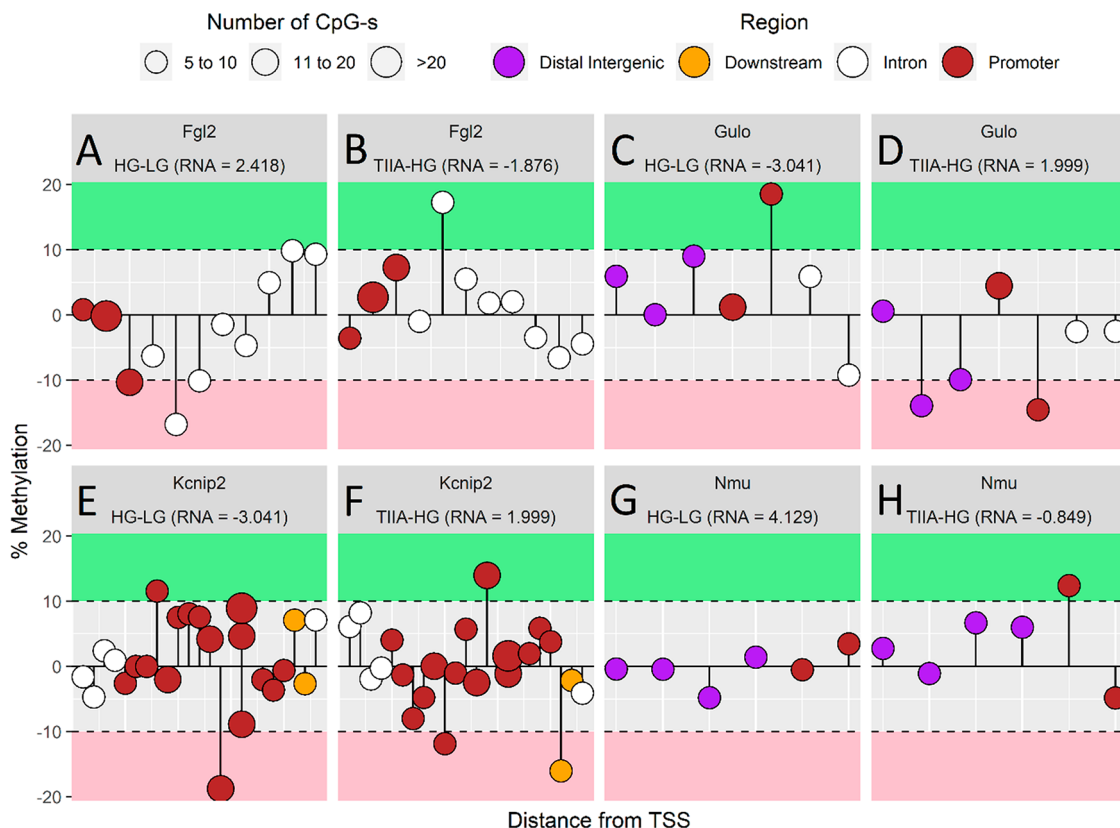


**Figure 7.** In-depth analysis of DNA methylation of *Fgl2* (A, B), *Gulo* (C, D), *Kcnip2* (E, F), and *Nmu* (G, H) as a lollipop plot. The length of the stems corresponds to the methylation ratio, up or down orientation indicates the increase or decrease of methylation, the area of the bubbles correlates to the number of CpGs of each CpG cluster, and the color of the bubbles codes for the different methylation regions (distal intergenic region: purple; downstream: yellow; intron: white; promoter: red). RNA expressions of genes of interest are also listed in the figure.

trienes, prostaglandin, and other chemicals, which can be subsequently degraded by  $\gamma$ -glutamyl hydrolase or  $\gamma$ -glutamyl transpeptidase, and dipeptidases.<sup>52</sup> Our findings suggest TIIA treatment can restore the cellular response induced by HG mainly targeting the above two pathways.

The tox analysis by IPA is to indicate most associated biological processes and toxicological responses to xenobiotic influence. In the top 10 mostly associated tox changes (Figure 9), the majority of toxicological responses in HG/LG and TIIA/HG are both mainly associated with kidney disorders, which suggest the suitability of high-glucose-induced mes-13 cell model as an in vitro DN cell model. In Figure 10, the most associated disease types, both HG/LG and TIIA/HG models are highly associated with endocrine system disorders and organism injuries, which correlate well with DN.

**Correlated Genes of Interest.** On the basis of the analysis of SureSelect-methy-seq and RNA-seq results and correlation with clinical pathological changes, we identified four most relevant genes, in which HG can induce DN pathological associated changes in gene expression and accompanying with an opposite DNA methylation change in DNA promoter, while TIIA can restore the alteration to normal.

NMU, a neuropeptide that belongs to the neuromedin family, can generate active neuropeptides and regulate pain, stress, cancer, and inflammatory diseases.<sup>53</sup> Recent findings indicate that NMU can act directly on pancreas  $\beta$  cells through NMUR1 in an autocrine or paracrine fashion to suppress insulin secretion.<sup>54</sup> In our in vitro system, HG can induce a very according high *Nmu* expression fold change (17.495) over

LG, which is the highest fold change in HG/LG comparison (Table 4) accompanying with a decrease in DNA methylation ( $-0.526$ ) of *Nmu* promoter, which suggests increase of *Nmu* by HG correlates with the decrease of DNA methylation in its promoter region. TIIA can reverse the change in gene expression and DNA methylation and indicate the potential therapeutic target on *Nmu*. Fibrinogen-like protein 2 (FGL2) is a novel prothrombinase. Increased *Fgl2* level was found to be highly correlated with the circulating TNF- $\alpha$  levels and severity of mouse type 2 diabetic nephropathy.<sup>55</sup> Like *Nmu*, HG can induce a very according high *Fgl2* expression fold change (5.346) over LG accompanying with a decrease in DNA methylation ( $-10.324$ ) of *Nmu* promoter. TIIA treatment also demonstrates a relative restoration effect on both gene expression and DNA methylation.

Ascorbic acid can promote Ten-Eleven Translocation (TET) mediated 5-methylcytosine oxidation and DNA demethylation.<sup>56</sup> In rodents, L-gulono- $\gamma$ -lactone oxidase (GLO) is necessary for synthesis of ascorbic acid and was found to be decreased in diabetic rats.<sup>57</sup> However, this might not occur in human cells, since humans cannot synthesize ascorbic acid by themselves due to an inherited mutation in GLO gene.<sup>58</sup>

In a Type 2 rat diabetes model, potassium voltage-gated channel interacting protein 2 (KCNIP2/KChIP2) was found to be down-regulated.<sup>58</sup> Our results (Table 4) echo the above findings that HG can decrease *Glo* and *Kcnip2* greatly (both 0.121) and correlate with an increase in the methylation ratio in their promoters (18.530 and 11.567, respectively). TIIA can

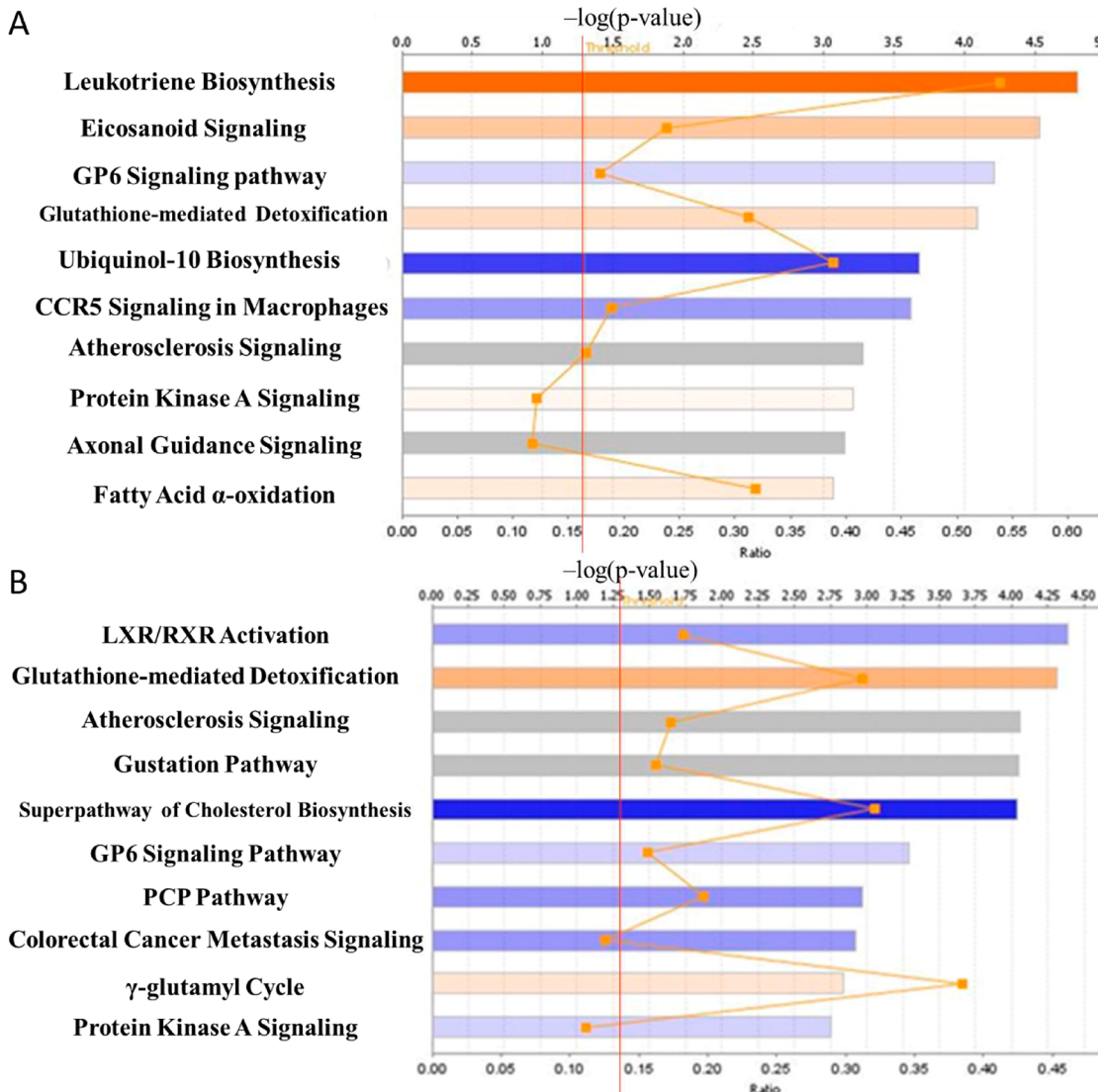


**Figure 8.** Canonical pathways identified by IPA for all significant and reliable differentially expressed genes in HG versus LG (A) and TIIA versus HG (B) from mes-13 cells after 5 d treatment. Canonical pathways are displayed as the $-\log(p\text{-value})$  with the threshold of 1.3 indicating the minimum significance level. Length of the bars represents the significant associations.

effectively reverse the alteration in both gene expression and DNA methylation.

Those four genes of interest will be targets for our further investigation.

Others have reported that diabetes could induce hypermethylation and hypomethylation of different genes at same time. For instance, in genomic DNA of whole blood from diabetes patients, 153 loci showed hypomethylation, and 225 showed hypermethylation.<sup>59</sup> Additionally, high-glucose environment increased thrombospondin-1 expression in keratinocytes via DNA hypomethylation.<sup>60</sup> High glucose also decreases BDNF in RSC96 cells by DNA hypermethylation of BDNF promoters.<sup>61</sup> However, the clear and underlying mechanism for whole genome methylation alterations remains unknown. In our previous reported study, TIIA can modulate DNMTs and HDACs activities.<sup>19</sup> TIIA may also have the potential to modulate TET function. With the above assumptions, TIIA may modulate methylation in specific CpGs and restore some of the methylation changes induced by high glucose. Although TIIA has proven its therapeutic effects on diabetic nephropathy,<sup>24,31</sup> our research is the first attempt to explore the

potential restoration effects of TIIA in diabetic nephropathy model epigenomically. The next goal is to investigate the underlined methylation modulation mechanisms.

In conclusion, our current study demonstrated the TIIA protective effect against HG-induced damage to kidney. Using SureSelect Methyl-seq and RNA-seq, we provided a quantitative global profile of the methylome and transcriptome in mouse kidney mesangial cells from LG and HG with or without TIIA treatments. IPA analysis identified inflammation pathways like leukotriene biosynthesis and eicosanoid signaling were activated by HG stimulation, while TIIA treatment may enhance glutathione-mediated detoxification pathway to overcome the resulting excess oxidative stress and inflammation. Importantly, we identified that DNA methylation of a list of DN associated genes, *Nmu*, *Fgl2*, *Glo*, and *Kcnip2*, were altered in HG-induced DN model and that TIIA treatment effectively restored the DNA methylation and gene expression. These findings could potentially provide novel insights into the understanding of how epigenetic modifications affect the progression of DN and the preventive effect of TIIA.

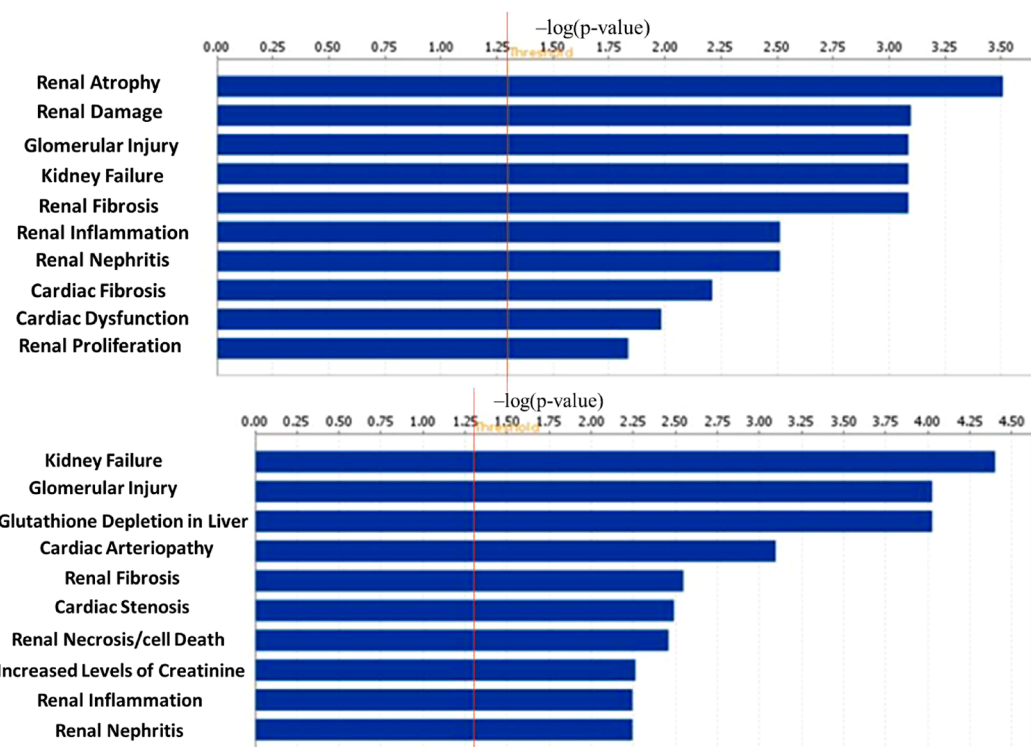


**Figure 9.** 10 most associated tox results identified by IPA related to HG vs LG (upper) and TIIA vs HG (lower) from mes-13 cells after 5 d treatment. The tox analysis applies toxicity functions together with toxicity lists to connect experimental findings to clinical pathology and to understand pharmacological response. IPA tox results are displayed as the  $-\log(p\text{-value})$  with the threshold of 1.3 indicating the minimum significance level. Length of the bars represents the significant associations.

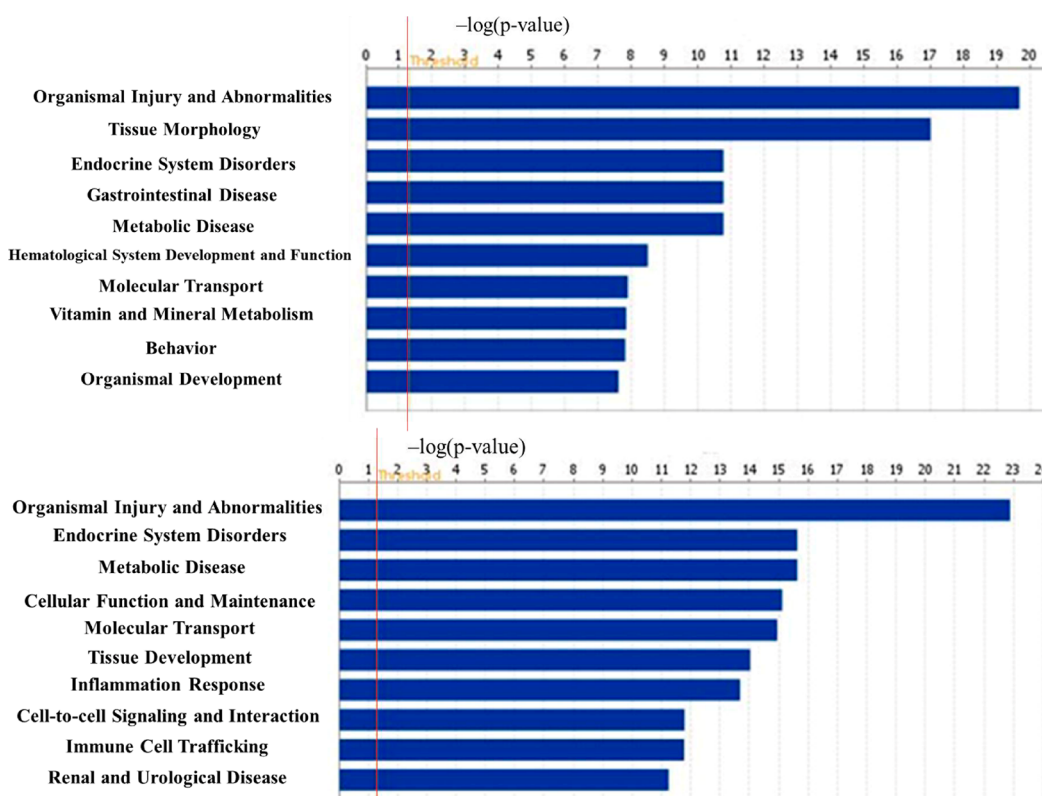


**Figure 10.** 10 most associated diseases related to HG vs LG (upper) and TIIA vs HG (lower) with the threshold of 1.3 ( $-\log(p\text{-value})$ ) indicating the minimum significance level. IPA provides association between experimental results to clinical disease to find the most associated disease types. Both HG/LG and TIIA/HG models are highly associated with endocrine system disorders and organism injuries, which correlate well with DN.

## ASSOCIATED CONTENT

### Supporting Information

The Supporting Information is available free of charge on the ACS Publications website at DOI: [10.1021/acs.chemrestox.9b00117](https://doi.org/10.1021/acs.chemrestox.9b00117).

Differentially expressed genes in two comparisons among three groups (HG/LG and TIIA/HG), and heatmap indicating methylation ratio of promoter, gene body, and downstream regions comparison between LG, HG, and TIIA from SureSelect Methyl-seq results at the individual gene level ([PDF](#))

## AUTHOR INFORMATION

### Corresponding Author

\*Phone: 732-455-3831. Fax: 732-455-3134. E-mail: KongT@pharmacy.rutgers.edu.

### ORCID

Ah-Ng Kong: [0000-0002-9273-4217](#)

### Author Contributions

<sup>†</sup>Equal contribution.

### Notes

The authors declare no competing financial interest.

## ACKNOWLEDGMENTS

This work was supported in part by institutional funds and by R01-AT007065 from NCCIH and the Office of Dietary Supplements. The authors express sincere gratitude to all members of Dr. T. Kong's laboratory for their helpful discussions.

## REFERENCES

- (1) Cooper, M. E. (1998) Pathogenesis, prevention, and treatment of diabetic nephropathy. *Lancet* 352, 213–219.
- (2) Nguyen, D. V., Shaw, L. C., and Grant, M. B. (2012) Inflammation in the pathogenesis of microvascular complications in diabetes. *Front. Endocrinol. (Lausanne, Switz.)* 3, 170.
- (3) Sharma, I., Dutta, R. K., Singh, N. K., and Kanwar, Y. S. (2017) High Glucose-Induced Hypomethylation Promotes Binding of Sp-1 to Myo-Inositol Oxygenase: Implication in the Pathobiology of Diabetic Tubulopathy. *Am. J. Pathol.* 187, 724–739.
- (4) Abdo, S., Zhang, S. L., and Chan, J. S. (2015) Reactive Oxygen Species and Nuclear Factor Erythroid 2-Related Factor 2 Activation in Diabetic Nephropathy: A Hidden Target. *J. Diabetes Metab.* 6. DOI: [10.4172/2155-6156.1000547](https://doi.org/10.4172/2155-6156.1000547)
- (5) Han, Y., Xu, X., Tang, C., Gao, P., Chen, X., Xiong, X., Yang, M., Yang, S., Zhu, X., Yuan, S., Liu, F., Xiao, L., Kanwar, Y. S., and Sun, L. (2018) Reactive oxygen species promote tubular injury in diabetic nephropathy: The role of the mitochondrial ros-txnip-nlrp3 biological axis. *Redox Biol.* 16, 32–46.
- (6) Fridlyand, L. E., and Philipson, L. H. (2005) Oxidative reactive species in cell injury: Mechanisms in diabetes mellitus and therapeutic approaches. *Ann. N. Y. Acad. Sci.* 1066, 136–151.
- (7) Kiritoshi, S., Nishikawa, T., Sonoda, K., Kukidome, D., Senokuchi, T., Matsuo, T., Matsumura, T., Tokunaga, H., Brownlee, M., and Araki, E. (2003) Reactive oxygen species from mitochondria induce cyclooxygenase-2 gene expression in human mesangial cells: potential role in diabetic nephropathy. *Diabetes* 52, 2570–2577.
- (8) Koya, D., Hayashi, K., Kitada, M., Kashiwagi, A., Kikkawa, R., and Haneda, M. (2003) Effects of antioxidants in diabetes-induced oxidative stress in the glomeruli of diabetic rats. *J. Am. Soc. Nephrol.* 14, 250S–253.
- (9) Yamamoto, T., Nakamura, T., Noble, N. A., Ruoslahti, E., and Border, W. A. (1993) Expression of transforming growth factor beta is elevated in human and experimental diabetic nephropathy. *Proc. Natl. Acad. Sci. U. S. A.* 90, 1814–1818.
- (10) Bakin, A. V., Stourman, N. V., Sekhar, K. R., Rinehart, C., Yan, X., Meredith, M. J., Arteaga, C. L., and Freeman, M. L. (2005) Smad3-ATF3 signaling mediates TGF-beta suppression of genes encoding Phase II detoxifying proteins. *Free Radical Biol. Med.* 38, 375–387.
- (11) Zhang, D. D. (2006) Mechanistic studies of the Nrf2-Keap1 signaling pathway. *Drug Metab. Rev.* 38, 769–789.
- (12) Li, W., Guo, Y., Zhang, C., Wu, R., Yang, A. Y., Gaspar, J., and Kong, A. N. (2016) Dietary Phytochemicals and Cancer Chemoprevention: A Perspective on Oxidative Stress, Inflammation, and Epigenetics. *Chem. Res. Toxicol.* 29, 2071–2095.
- (13) Lee, J. H., Khor, T. O., Shu, L., Su, Z. Y., Fuentes, F., and Kong, A. N. (2013) Dietary phytochemicals and cancer prevention: Nrf2 signaling, epigenetics, and cell death mechanisms in blocking cancer initiation and progression. *Pharmacol. Ther.* 137, 153–171.
- (14) Bahadoran, Z., Mirmiran, P., and Azizi, F. (2013) Potential efficacy of broccoli sprouts as a unique supplement for management of type 2 diabetes and its complications. *J. Med. Food* 16, 375–382.
- (15) Jimenez-Osorio, A. S., Gonzalez-Reyes, S., and Pedraza-Chaverri, J. (2015) Natural Nrf2 activators in diabetes. *Clin. Chim. Acta* 448, 182–192.
- (16) Zheng, H., Whitman, S. A., Wu, W., Wondrak, G. T., Wong, P. K., Fang, D., and Zhang, D. D. (2011) Therapeutic potential of Nrf2 activators in streptozotocin-induced diabetic nephropathy. *Diabetes* 60, 3055–3066.
- (17) Xu, S., and Liu, P. (2013) Tanshinone II-A: new perspectives for old remedies. *Expert Opin. Ther. Pat.* 23, 149–153.
- (18) An, L., Peng, L. Y., Sun, N. Y., Yang, Y. L., Zhang, X. W., Li, B., Liu, B. L., Li, P., and Chen, J. (2019) Tanshinone IIA Activates Nuclear Factor-Erythroid 2-Related Factor 2 to Restrain Pulmonary Fibrosis via Regulation of Redox Homeostasis and Glutaminolysis. *Antioxid. Redox Signaling* 30, 1831.
- (19) Wang, L., Zhang, C., Guo, Y., Su, Z. Y., Yang, Y., Shu, L., and Kong, A. N. (2014) Blocking of JB6 cell transformation by tanshinone IIA: epigenetic reactivation of Nrf2 antioxidative stress pathway. *AAPS J.* 16, 1214–1225.
- (20) Cai, M., Guo, Y., Wang, S., Wei, H., Sun, S., Zhao, G., and Dong, H. (2017) Tanshinone IIA Elicits Neuroprotective Effect Through Activating the Nuclear Factor Erythroid 2-Related Factor-Dependent Antioxidant Response. *Rejuvenation Res.* 20, 286–297.
- (21) Sui, H., Zhao, J., Zhou, L., Wen, H., Deng, W., Li, C., Ji, Q., Liu, X., Feng, Y., Chai, N., Zhang, Q., Cai, J., and Li, Q. (2017) Tanshinone IIA inhibits beta-catenin/VEGF-mediated angiogenesis by targeting TGF-beta1 in normoxic and HIF-1alpha in hypoxic microenvironments in human colorectal cancer. *Cancer Lett.* 403, 86–97.
- (22) Gao, H., Huang, L., Ding, F., Yang, K., Feng, Y., Tang, H., Xu, Q., M., Feng, J., and Yang, S. (2018) Simultaneous purification of dihydrotanshinone, tanshinone I, cryptotanshinone, and tanshinone IIA from Salvia miltiorrhiza and their anti-inflammatory activities investigation. *Sci. Rep.* 8, 8460.
- (23) Liu, T., Jin, H., Sun, Q. R., Xu, J. H., and Hu, H. T. (2010) The neuroprotective effects of tanshinone IIA on beta-amyloid-induced toxicity in rat cortical neurons. *Neuropharmacology* 59, 595–604.
- (24) Chen, X., Wu, R., Kong, Y., Yang, Y., Gao, Y., Sun, D., Liu, Q., Dai, D., Lu, Z., Wang, N., Ge, S., and Wang, F. (2017) Tanshinone IIA attenuates renal damage in STZ-induced diabetic rats via inhibiting oxidative stress and inflammation. *Oncotarget* 8, 31915–31922.
- (25) Fan, K., Li, S., Liu, G., Yuan, H., Ma, L., and Lu, P. (2017) Tanshinone IIA inhibits high glucose-induced proliferation, migration and vascularization of human retinal endothelial cells. *Mol. Med. Rep.* 16, 9023–9028.
- (26) Jiang, C., Zhu, W., Shao, Q., Yan, X., Jin, B., Zhang, M., and Xu, B. (2016) Tanshinone IIA Protects Against Folic Acid-Induced Acute Kidney Injury. *Am. J. Chin. Med.* 44, 737–753.

- (27) Jiang, C., Zhu, W., Yan, X., Shao, Q., Xu, B., Zhang, M., and Gong, R. (2016) Rescue therapy with Tanshinone IIA hinders transition of acute kidney injury to chronic kidney disease via targeting GSK3beta. *Sci. Rep.* 6, 36698.
- (28) Ahn, Y. M., Kim, S. K., Lee, S. H., Ahn, S. Y., Kang, S. W., Chung, J. H., Kim, S. D., and Lee, B. C. (2010) Renoprotective effect of Tanshinone IIA, an active component of Salvia miltiorrhiza, on rats with chronic kidney disease. *Phytother. Res.* 24, 1886–1892.
- (29) Jiang, C., Shao, Q., Jin, B., Gong, R., Zhang, M., and Xu, B. (2015) Tanshinone IIA Attenuates Renal Fibrosis after Acute Kidney Injury in a Mouse Model through Inhibition of Fibrocytes Recruitment. *BioMed Res. Int.* 2015, 867140.
- (30) Chen, G., Zhang, X., Li, C., Lin, Y., Meng, Y., and Tang, S. (2014) Role of the TGF $\beta$ /p65 pathway in tanshinone A-treated HBZY1 cells. *Mol. Med. Rep.* 10, 2471–2476.
- (31) Kim, S. K., Jung, K. H., and Lee, B. C. (2009) Protective effect of Tanshinone IIA on the early stage of experimental diabetic nephropathy. *Biol. Pharm. Bull.* 32, 220–224.
- (32) Hadden, M. J., and Advani, A. (2018) Histone Deacetylase Inhibitors and Diabetic Kidney Disease. *Int. J. Mol. Sci.* 19, 2630.
- (33) Keating, S. T., van Diepen, J. A., Riksen, N. P., and El-Osta, A. (2018) Epigenetics in diabetic nephropathy, immunity and metabolism. *Diabetologia* 61, 6–20.
- (34) Leti, F., Morrison, E., and DiStefano, J. K. (2017) Long noncoding RNAs in the pathogenesis of diabetic kidney disease: implications for novel therapeutic strategies. *Pers. Med.* 14, 271–278.
- (35) Long, J., Badal, S. S., Ye, Z., Wang, Y., Ayanga, B. A., Galvan, D. L., Green, N. H., Chang, B. H., Overbeek, P. A., and Danesh, F. R. (2016) Long noncoding RNA Tug1 regulates mitochondrial bioenergetics in diabetic nephropathy. *J. Clin. Invest.* 126, 4205–4218.
- (36) Rubin, A., Salzberg, A. C., Imamura, Y., Grivitishwilli, A., and Tombran-Tink, J. (2016) Identification of novel targets of diabetic nephropathy and PEDF peptide treatment using RNA-seq. *BMC Genomics* 17, 936.
- (37) Andrews, S. (2010) *FastQC: a quality control tool for high throughput sequence data*. Online at <https://www.bioinformatics.babraham.ac.uk/projects/fastqc/>.
- (38) Li, H., Handsaker, B., Wysoker, A., Fennell, T., Ruan, J., Homer, N., Marth, G., Abecasis, G., and Durbin, R. (2009) The Sequence Alignment/Map format and SAMtools. *Bioinformatics* 25, 2078–2079.
- (39) Kim, D., Langmead, B., and Salzberg, S. L. (2015) HISAT: a fast spliced aligner with low memory requirements. *Nat. Methods* 12, 357–360.
- (40) Krueger, F., and Andrews, S. R. (2011) Bismark: a flexible aligner and methylation caller for Bisulfite-Seq applications. *Bioinformatics* 27, 1571–1572.
- (41) Team, R. C. (2013) *R: A language and environment for statistical computing*. Online at <https://www.gbif.org/tool/81287/r-a-language-and-environment-for-statistical-computing>
- (42) Wang, L., Feng, Z., Wang, X., Wang, X., and Zhang, X. (2010) DEGseq: an R package for identifying differentially expressed genes from RNA-seq data. *Bioinformatics* 26, 136–138.
- (43) Storey, J. D. (2003) The positive false discovery rate: a Bayesian interpretation and the q-value. *Annals of Statistics* 31, 2013–2035.
- (44) Gaspar, J. M., and Hart, R. P. (2017) DMRfinder: efficiently identifying differentially methylated regions from MethylC-seq data. *BMC Bioinf.* 18, 528.
- (45) Yu, G., Wang, L. G., and He, Q. Y. (2015) ChIPseeker: an R/Bioconductor package for ChIP peak annotation, comparison and visualization. *Bioinformatics* 31, 2382–2383.
- (46) Zhou, S., Treloar, A. E., and Lupien, M. (2016) Emergence of the Noncoding Cancer Genome: A Target of Genetic and Epigenetic Alterations. *Cancer Discovery* 6, 1215–1229.
- (47) Wenzel, S. E. (1997) Arachidonic acid metabolites: mediators of inflammation in asthma. *Pharmacotherapy* 17, 3S–12S.
- (48) Peters-Golden, M., Canetti, C., Mancuso, P., and Coffey, M. J. (2005) Leukotrienes: underappreciated mediators of innate immune responses. *J. Immunol.* 174, 589–594.
- (49) Smyth, E. M., and Fitzgerald, G. A. (2009) The eicosanoids: prostaglandins, thromboxanes, leukotrienes, and related compounds. *Basic and clinical pharmacology*. 12th ed.; McGraw Hill Medical, 313–329.
- (50) Smyth, E. M., Grosser, T., Wang, M., Yu, Y., and Fitzgerald, G. A. (2009) Prostanoids in health and disease. *J. Lipid Res.* 50, S423–S428.
- (51) Makishima, M. (2005) Nuclear receptors as targets for drug development: regulation of cholesterol and bile acid metabolism by nuclear receptors. *J. Pharmacol. Sci.* 97, 177–183.
- (52) Burg, D., and Mulder, G. J. (2002) Glutathione conjugates and their synthetic derivatives as inhibitors of glutathione-dependent enzymes involved in cancer and drug resistance. *Drug Metab. Rev.* 34, 821–863.
- (53) Budhiraja, S., and Chugh, A. (2009) Neuromedin U: physiology, pharmacology and therapeutic potential. *Fundam. Clin. Pharmacol.* 23, 149–157.
- (54) Zhang, W., Sakoda, H., Miura, A., Shimizu, K., Mori, K., Miyazato, M., Takayama, K., Hayashi, Y., and Nakazato, M. (2017) Neuromedin U suppresses glucose-stimulated insulin secretion in pancreatic  $\beta$  cells. *Biochem. Biophys. Res. Commun.* 493, 677–683.
- (55) Su, G., Liu, K., Wang, Y., Wang, J., Li, X., Li, W., Liao, Y., and Wang, Z. (2011) Fibrinogen-like protein 2 expression correlates with microthrombosis in rats with type 2 diabetic nephropathy. *J. Biomed. Res.* 25, 120–127.
- (56) Yin, R., Mao, S. Q., Zhao, B., Chong, Z., Yang, Y., Zhao, C., Zhang, D., Huang, H., Gao, J., Li, Z., Jiao, Y., Li, C., Liu, S., Wu, D., Gu, W., Yang, Y. G., Xu, G. L., and Wang, H. (2013) Ascorbic acid enhances Tet-mediated 5-methylcytosine oxidation and promotes DNA demethylation in mammals. *J. Am. Chem. Soc.* 135, 10396–10403.
- (57) Kashiba, M., Oka, J., Ichikawa, R., Kasahara, E., Inayama, T., Kageyama, A., Kageyama, H., Osaka, T., Umegaki, K., Matsumoto, A., Ishikawa, T., Nishikimi, M., Inoue, M., and Inoue, S. (2002) Impaired ascorbic acid metabolism in streptozotocin-induced diabetic rats. *Free Radical Biol. Med.* 33, 1221–1230.
- (58) Sato, T., Kobayashi, T., Kuno, A., Miki, T., Tanno, M., Kouzu, H., Itoh, T., Ishikawa, S., Kojima, T., Miura, T., and Tohse, N. (2014) Type 2 diabetes induces subendocardium-predominant reduction in transient outward K<sup>+</sup> current with downregulation of Kv4.2 and KCNIP2. *Am. J. Physiol Heart Circ Physiol* 306, H1054–1065.
- (59) Chen, Z., Miao, F., Paterson, A. D., Lachin, J. M., Zhang, L., Schones, D. E., Wu, X., Wang, J., Tompkins, J. D., Genuth, S., Braffett, B. H., Riggs, A. D., and Natarajan, R. (2016) Epigenomic profiling reveals an association between persistence of DNA methylation and metabolic memory in the DCCT/EDIC type 1 diabetes cohort. *Proc. Natl. Acad. Sci. U. S. A.* 113, E3002–3011.
- (60) Lan, C. C., Huang, S. M., Wu, C. S., Wu, C. H., and Chen, G. S. (2016) High-glucose environment increased thrombospondin-1 expression in keratinocytes via DNA hypomethylation. *Transl. Res.* 169, 91–101. e101–103.
- (61) Zhang, C. H., Lv, X., Du, W., Cheng, M. J., Liu, Y. P., Zhu, L., and Hao, J. (2019) The Akt/mTOR cascade mediates high glucose-induced reductions in BDNF via DNMT1 in Schwann cells in diabetic peripheral neuropathy. *Exp. Cell Res.* 383, 111502.